

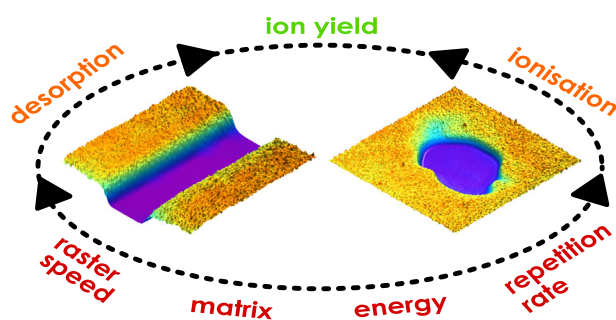
# The Influence of MS Imaging Parameters on UV-MALDI Desorption and Ion Yield

Kenneth N. Robinson,<sup>1,2</sup> Rory T. Steven,<sup>1</sup> Alan M. Race,<sup>1</sup> Josephine Bunch<sup>1,3</sup>

<sup>1</sup>National Centre of Excellence in Mass Spectrometry Imaging (NiCE-MSI), National Physical Laboratory, Teddington, UK

<sup>2</sup>Advanced Materials and Healthcare Technologies Division (AMHT), University of Nottingham, Nottingham, UK

<sup>3</sup>Department of Surgery and Cancer, Faculty of Medicine, Imperial College London, London, UK



**Abstract.** Ultraviolet matrix-assisted laser desorption/ionization mass spectrometry imaging (UV-MALDI MSI) is a widely used technique for imaging molecular distributions within biological systems. While much work exists concerning desorption in UV-MALDI MS, the effects of commonly varied parameters for imaging applications (repetition rate, use of continuous raster mode and raster speed), which determine spatial resolution and limits of detection for the technique,

remain largely unknown. We use multiple surface characterization modalities to obtain quantitative measurements of material desorption and analyte ion yield in thin film model systems of two matrix compounds, arising from different UV-MALDI MSI sampling conditions. Observed changes in resulting ablation feature point to matrix-dependent spatial resolution and laser-induced matrix modification effects. Analyte ion yields of  $10^{-9}$  to  $10^{-6}$  are observed. Complex changes in ion yield, between spot and raster sampling and arising from varied laser repetition rate and raster speed, are observed.

**Keywords:** MALDI, MSI, Ionization, Desorption

Received: 16 November 2018/Revised: 12 February 2019/Accepted: 11 March 2019/Published Online: 4 April 2019

## Introduction

Ultraviolet matrix-assisted laser desorption/ionization mass spectrometry imaging (UV-MALDI MSI) is an analytical technique used for imaging the molecular distributions of a wide array of compounds, most commonly pharmaceuticals, bio-molecules, and polymers [1–3]. This capability has seen the technique utilized in a variety of research areas, most notably in biomedical research fields such as drug development, molecular biology, and pathology [1, 4–6].

The ejection of material, resulting from the interaction between the matrix, the sample, and the laser, is one of the key steps of the UV-MALDI process, and as such will have a strong influence on UV-MALDI MSI data. Widely described as “desorption” in literature, the ejection of material from a sample surface in a typical UV-MALDI MS experiment can, in fact, involve either a steady release of molecules from the solid matrix into the gas phase (desorption) or a rapid disintegration of the matrix into clusters and free molecules (ablation), or a combination of the two [7, 8].

Material ejection in UV-MALDI MS has been extensively studied [7], with two primary mechanisms, phase explosion [9] and quasi-thermal desorption [10], proposed to describe the ablation and desorption processes respectively. Under typical UV-MALDI MS conditions, both mechanisms are expected to occur [11], with a recent study by Niehaus et al. showing evidence that quasi-thermal desorption occurs at low laser fluences until a certain threshold is reached, above which

**Electronic supplementary material** The online version of this article (<https://doi.org/10.1007/s13361-019-02193-8>) contains supplementary material, which is available to authorized users.

Correspondence to: Rory Steven; e-mail: rory.steven@npl.co.uk, Josephine Bunch; e-mail: josephine.bunch@npl.co.uk

ablative processes like phase explosion dominate [8]. Additional factors such as pulse width [9], wavelength [10], and matrix characteristics [12] are also believed to favor one mechanism over the other. Generally speaking, desorption and ablation are favored by either slow or rapid introduction of energy into the matrix respectively.

Studies into material ejection in UV-MALDI MS typically measure the resulting desorption plume or sample surface effects. Characterization of UV-MALDI desorption plumes has been reported via laser-induced fluorescence (LIF) [13], fast flash imaging [14], shadowgraphy [15], and laser post ionization [8]. Measurements of the spatial distribution of ions within UV-MALDI plumes have also been reported using custom rotatable TOF MS systems [16] and spatially sensitive ion detectors [17]. Investigations into laser-induced surface effects most commonly make use of light microscopy and secondary electron microscopy (SEM) [18–24], which are typically used to measure ablation spot diameters and study morphological changes to the matrix. Despite the widespread use of volumetric measurements in laser ablation studies [11], there have been surprisingly few examples of such measurements related to UV-MALDI MS, with only two measurements of crater volumes, via profilometry [24] and confocal laser scanning microscopy (CLSM) [25], being reported.

The topic of ion yields, the ratio of formed ions to a total number of ejected molecules, in UV-MALDI MS has received significant attention in recent years. A series of studies originating from the Kim [26, 27] and Ni groups [28] proposed that the absolute magnitudes of ion yields in UV-MALDI MS are orders of magnitude lower than the previously accepted values. This had important implications for UV-MALDI MS ionization theories, leading to a lively debate on the matter [26–36]. Although the controversial nature of absolute ion yields was seemingly resolved [36], there still remains some disagreement on the matter [37].

Investigations into the influence of UV-MALDI MS experimental conditions on ion yield have been typically focused on basic parameters such as laser fluence, analyte molar ratios, and choice of matrix compound. The role of laser wavelength on relative ion yields has been investigated through correlation of ion signals with acoustic measurements of mass removal [10], although as these experiments were conducted at atmospheric pressures, the applicability to the vacuum environment found in typical UV-MALDI MS instruments is unknown. Pulse width has also been investigated in molecular dynamic simulations [9] and experimentally [38, 39].

Parameters relevant to UV-MALDI MSI, such as laser repetition rate, spot size, sampling mode, and raster speed, have received significant attention in recent years [40–43]. These studies have thus far been limited to investigating the impact on detected ion intensities; therefore, a study into how common imaging acquisition parameters can affect material ejection and absolute ion yields is clearly of interest.

Here, we utilize uniform, well-characterized thin film model systems consisting of known quantities of the pharmaceutical olanzapine, combined the matrix compounds  $\alpha$ -cyano-4-

hydroxycinnamic acid (CHCA) and 2,5-dihydroxybenzoic acid (DHB), to explore the influence of laser pulse energy, repetition rate, and raster speed on material ejection and ion yield in UV-MALDI MSI experiments. We make use of atomic force microscopy (AFM), SEM, and CLSM as surface analysis tools to investigate material ejection in MSI experiments, providing insights into the effect of sampling mode and laser conditions on both spatial resolution and limit of detection. Measurements of material ejection are combined with the corresponding MS data to provide estimations of absolute ion yield under sampling and laser conditions relevant to UV-MALDI MSI.

## Materials

CHCA was purchased from Sigma Aldrich (Gillingham, UK). DHB and olanzapine ( $312.4 \text{ g mol}^{-1}$ ) were purchased from Alfa Aesar (Heysham, UK). Superfrost microscope slides for deposition substrates and HPLC grade methanol (MeOH) were purchased from Fischer Scientific (Loughborough, UK). AFM tips were purchased from NuNano (Bristol, UK). Deionized (DI) water ( $\rho = 15 \text{ M}\Omega\text{cm}^{-1}$ ) was generated by an Elga Purelab system (High Wycombe, UK).

## Methods

### *Sample Preparation*

Substrates were cleaned via 10 min sonication in MeOH followed DI water, and finally 15 min in a UV ozone cleaner (T10X10/OES, UVOCS, Lansdale, PA, USA).

Deposition of the analyte and matrix layers was carried out in an Auto 306 thermal evaporator (Edwards, Crawley, UK), operating at  $\sim 6 \times 10^{-6}$  mbar. A chilled block of copper ( $\sim 5^\circ\text{C}$ ) was used to cool the substrates, ensuring deposition of the compounds. Three-nanometer layers of olanzapine were deposited onto the substrates, followed by either CHCA (360 nm) or DHB (136 nm) layers. Resulting analyte:matrix ratios in the samples were 1:221 (CHCA) and 1:107 (DHB). The deposition was monitored via the evaporator's in-built quartz crystal microbalance (QCM) sensor.

### *UV-MALDI MS*

UV-MALDI MS data were acquired with a Synapt G2-Si qToF mass spectrometer (Waters, Manchester, UK), using the WREnS scripting tool (Waters, Manchester, UK) to automate variation of the sampling conditions during data collection. Positive mode MS data ( $m/z$  50–1500) were acquired in the mass spectrometer resolution mode, in both spot and raster mode, at five laser energies, two repetition rates, and two raster speeds. MS data were collected with a fixed scan time of 0.085 s, for the 500 Hz at 2000 Hz laser repetition rates used here; this corresponded to  $\sim 42$  and  $\sim 212$  pulses per spectra respectively. The laser pulse energy was monitored during the experiment by using partially reflecting mirror (BSF-10-UV,

Thorlabs, UK) to sample a portion of the beam and direct it towards a pyro-electric sensor (PD10-C, Ophir Photonics, USA). Post experiment measurements of the full beam energy were used to calibrate the experimental measurements. As the laser in the MALDI Synapt G2-Si (Nd:YAG DPPS, 355 nm, < 1.1 ns) had a Gaussian beam profile, laser spot size ranged from a minimum of  $119 \times 130 \mu\text{m}$  to maximum of  $194 \times 246 \mu\text{m}$  depending on pulse energy used, as measured from CHCA thin film via the fluorescence method [44]. The change in spot area with pulse energy is shown in Figure S1.

### Measurement of Material Ejection

AFM measurements were carried out using a MFP-3D-SA AFM (Asylum Research, High Wycombe, UK) operating in alternating contact (AC) mode.

CLSM imaging was carried out using a LEXT OLS4100 CLSM (Olympus, Southend-on-Sea, UK). A  $\times 50$  objective (MPLAPON50XLEXT, Olympus, Southend-on-Sea, UK) was used resulting in a  $256 \mu\text{m} \times 256 \mu\text{m}$  square field of view. This objective was used with a laser power setting of 36, to achieve the best obtainable depth resolution while preventing sample damage from the microscope's UV laser. For imaging features that were larger than the field of view, three stepped images were acquired for later tiling.

Electron microscopy images were acquired using a Supra 40 FE-SEM (Zeiss, Cambridge, UK) at 3 keV with a 20- $\mu\text{m}$  aperture and 14.3 mm working distance. Samples were coated with a layer of Au (approx. 2 nm) using a Q150T S sputter coater (Quorum Technologies, Laughton, UK) to reduce charging effects during imaging.

### Data Analysis

Unless stated otherwise, all data were processed in MATLAB (R2017a, MathWorks, Natick, MA, USA) and OriginPro 2016 (OriginLab, Northampton, MA, USA).

AFM and CLSM data were processed in SPIP (v6.6.3, Image Metrology, Denmark). Determination of crater boundaries was obtained with the software's Particle and Pore Analysis tool, using the Advanced Thresholding setting (Pore RMS factor = -1). Stitching of CLSM images was carried out in Gwyddion 2.48 [45].

MS data were converted into .imzML using imzMLConverter [46], and imported into MATLAB using SpectralAnalysis [47] for further processing and analysis. Spectral data underwent an interpolation re-binning process (bin size =  $m/z$  0.002) before peak intensities, taken as the integrated peak area at full width half maximum (FWHM), were extracted. MS data for olanzapine ion yield calculations were taken from the summed intensities of the  $[\text{M} + \text{H}]^+$ ,  $[\text{M} + \text{Na}]^+$ , and  $[\text{M} + \text{K}]^+$  ions, including all detected isotopic peaks. Ion intensities were converted to ion number using an average single ion intensity of 24 counts, as determined from electrospray experiments using leucine enkephalin ( $[\text{M} + \text{H}]^+ = m/z$  556.269), and corrected for the known transmission efficiency of the instrument ion optics (12.9%) and duty cycle of

the ToF pusher (10.2–10.9%). A more detailed description of the process can be found in the [Supplementary](#).

## Results

### Irradiation Effects

When seeking to determine the surface effects resulting from laser sampling in UV-MALDI, a variety of parameters are useful to measure. Firstly, knowledge of the initial matrix conditions is evidently important. Additionally, aspects of crater geometry (size, shape, volume) resulting from UV-MALDI MSI analysis can prove highly informative in determining factors influencing limits of detection and spatial resolution. Finally, chemical and physical modification of UV-MALDI matrices during laser irradiation has long been suspected to have an experimental impact; therefore, it is also advantageous to distinguish any changes to the matrix, be it to morphological or other properties.

AFM, SEM, and CLSM were used to characterize laser irradiation effects from the UV-MALDI MSI experiments (Figure 1); a summary of each technique can be found in Table S1. This overview is specific to instrumentation used here and is not a comment on the capabilities of the techniques as a whole.

SEM imaging of the pristine matrix films revealed significant differences in crystal shape between the matrix compounds (Figure 1a and d). Matching previous reports for sublimed films of the matrix compounds [48], CHCA films consisted of sub-micron-sized angular crystals, whereas the DHB films consisted of few micron long branched crystals.

In post laser irradiation, DHB showed a smoothing of crystal edges, becoming more apparent moving towards the center of the crater/raster trench, caused either through melting or sublimation (Figure 1d and f). Cone-like and ripple structures have been previously observed occurring after irradiation of large DHB crystal surfaces [21, 24], although this was not evident here, most likely due to differences in the sample studied. Craters in the CHCA film exhibited distinct morphological zones, with the angular matrix crystals gradually giving way to an amorphous porous surface, possibly evidencing a melting effect (Figure 1a and f). AFM images collected across these regions revealed distinct bands in the obtained phase map data (Figure 1b). AFM phase images, which shows changes in energy dissipation experienced by the AFM tip, act as an indicator of adhesion, viscoelasticity, and other material properties of a surface [49]. The bands, which correspond roughly to the zones observed in SEM (Figure 1a), therefore, may represent areas where the matrix has undergone modification by the laser. Phase maps for DHB revealed a gradual change (Figure 1e), also reflecting the SEM data for that matrix (Figure 1d).

Unidentified crystalline material, which was morphologically different from the pristine matrix, was observed in the central regions of DHB craters/raster trenches (Figure 1d and f). Due to surrounding regions being completely clear, re-



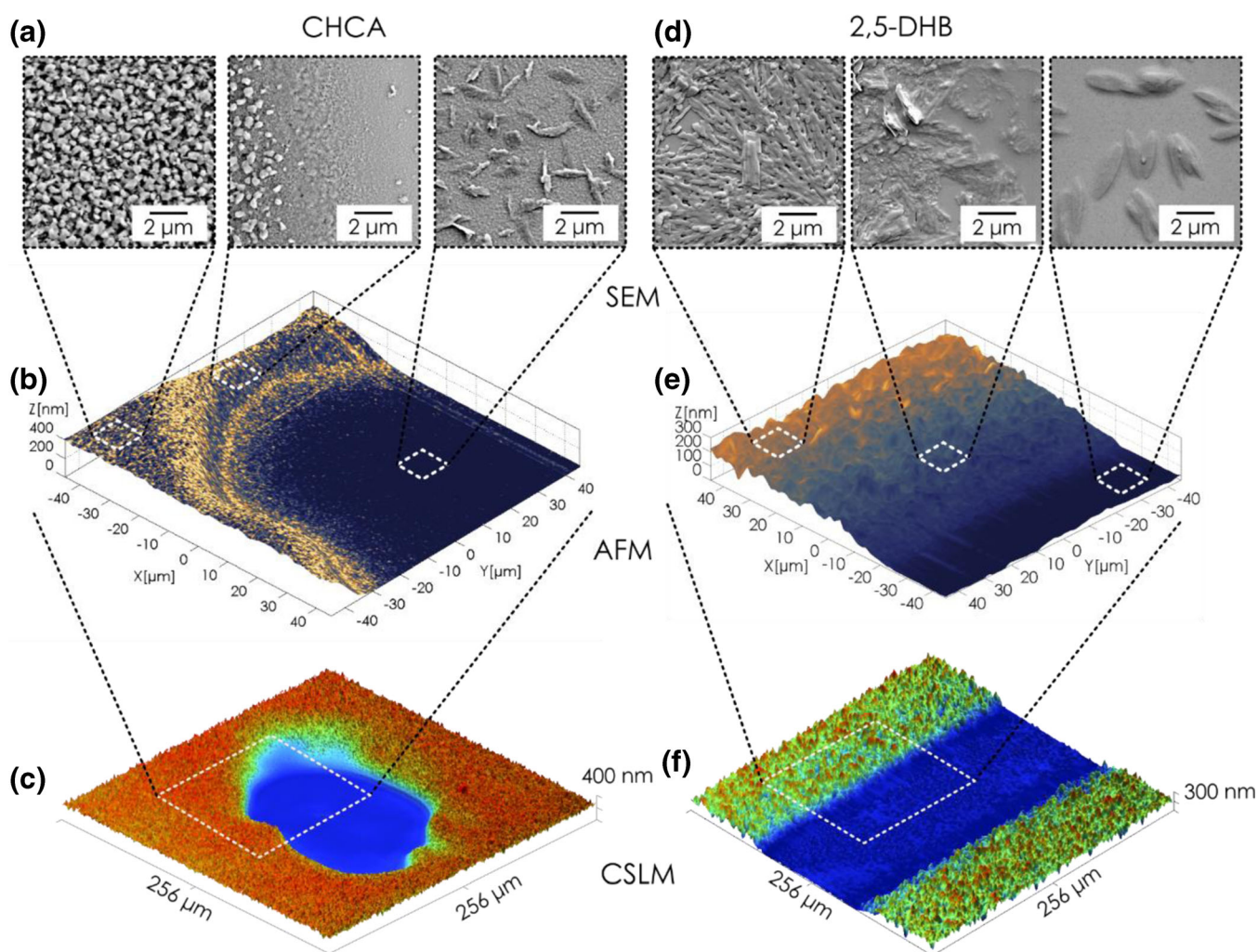


**Figure 1.** Surface analysis techniques for characterizing laser irradiation effects and material ejection in UV-MALDI MSI. (a) SEM images. (b) AFM topography image with a phase map overlay. (c) CSLM topographic image of a crater in CHCA film, resulting from spot mode acquisition, with a laser energy of 3.6 μJ and 500 Hz repetition rate. (d) SEM images. (e) AFM topography image with a phase map overlay. (f) CSLM topographic image of raster trench in DHB film, resulting from 2 mm/s raster mode acquisition, with a laser energy 7.3 μJ and 500 Hz repetition rate

deposition was presumed to be an unlikely source for this material. A similar effect was observed for CHCA, but with the material more uniformly distributed within the craters/raster trenches (Figure 1a and c). As there was no obvious visible evidence of redistribution on the surrounding matrix film, this material is presumed to be some sort of residue formed during laser irradiation.

Due to the large number of measurements required, and limitations of the SEM and AFM instruments (Table S1), CLSM was employed as the primary surface analysis technique to characterize material ejection resulting from the different studied UV-MALDI MSI experimental parameters.

### Characterizing Material Ejection in UV-MALDI MSI

Characterizing material ejection from a sample can provide valuable insight into many aspects of UV-MALDI MSI as it

impacts both limits of detection and spatial resolution of UV-MALDI MSI analyses. We used CLSM to characterize material ejection from model systems, consisting of a thin film of olanzapine with an overlayer of CHCA or DHB. The uniform nature of the samples enabled the craters/trenches formed under different UV-MALDI MSI sampling conditions to be accurately characterized. Figure 2 shows the changes in crater depth and size, material ejection, and olanzapine ion intensity over a range of laser pulse energies and repetition rates. Previously reported matrix density values [50] enabled material ejection, defined by the total number of molecules removed, to be estimated.

The intensity of olanzapine ( $I_{OLZ}$ ) increased with pulse energy (Figure 2c), reflecting the familiar relationship seen in UV-MALDI MS [50–53]. In contrast to the ion intensity data, the change in material ejection with pulse energy (Figure 2d) was much less pronounced, which is in agreement with previous reports showing significant deviations between material

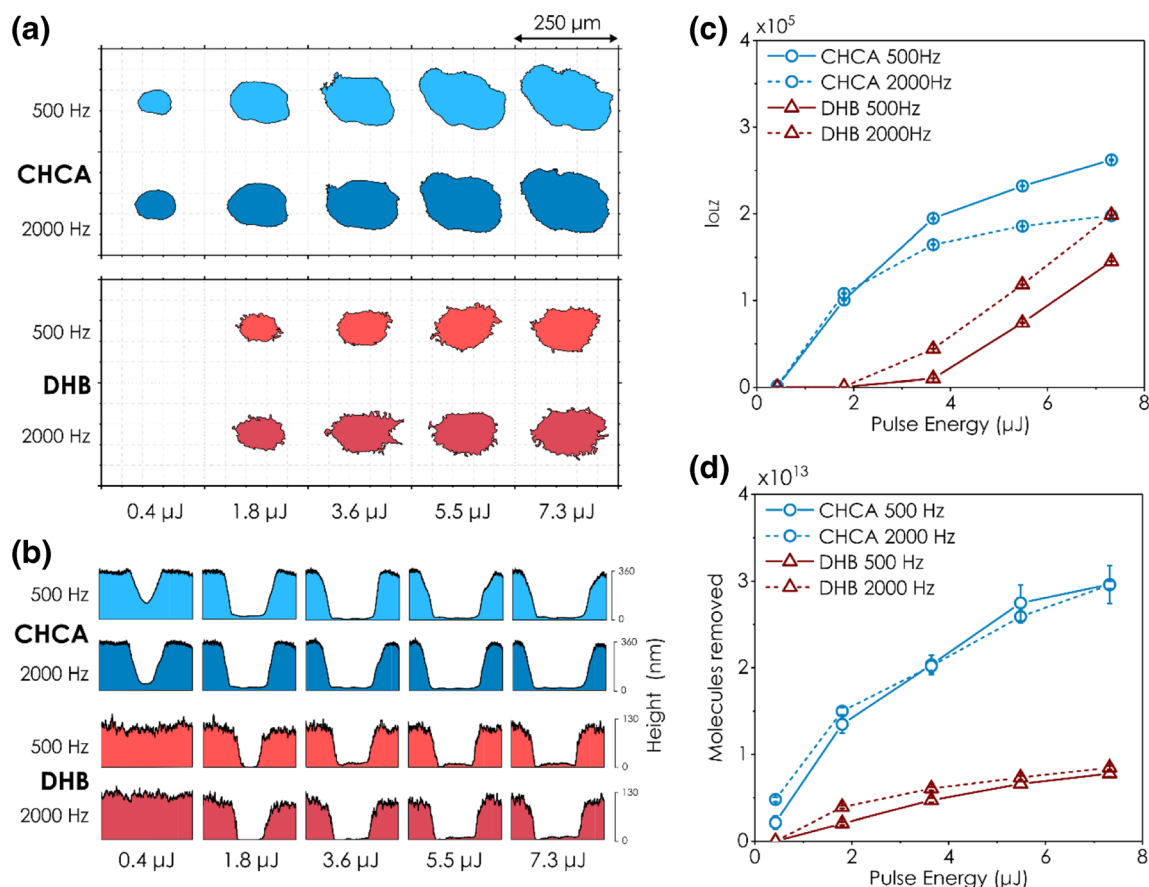


**Figure 2.** Ionization and material ejection from olanzapine + CHCA/DHB thin films in spot mode. **(a)** Averaged crater geometries ( $n = 5$ ). **(b)** Cross-sectional profiles of craters, at different pulse energies, and repetition rates, obtained from CLSM measurements. **(c)** Corresponding olanzapine ion intensities ( $I_{OLZ}$ ). Ion intensities are the summed values of  $\text{H}^+$ ,  $\text{Na}^+$ , and  $\text{K}^+$  adducts and all detected isotopic peaks. **(d)** Calculated number of molecules removed at different pulse energies and repetition rates from CLSM crater volume measurements. All error bars represent the expanded uncertainty ( $k = 2$ )

ejection and detected ion intensities [10, 24]. One distinguishing feature between desorption and ablation models in UV-MALDI is the relationship between laser energy and material ejection, with quasi-thermal desorption predicting an exponential relationship, and ablation either logarithmic or linear [7]. The evolution of material ejection with pulse energy (Figure 2d and Figure S2) appears to follow a logarithmic trend, suggesting that the ablation type processes are dominant. This agrees with previous studies that have placed this transition to ablation-like ejection mechanisms as coincident with the onset of significant ion generation [14, 54, 55]. On the other hand, photoacoustic measurements reported by the Dreisewerd group have shown that quasi-thermal desorption best describes material ejection at the laser energy range and spot size used here [8, 10]. The reason for this discrepancy is unknown, but may be due to the relatively short pulse width ( $\leq 1.1$  ns) and higher repetition rates (500 Hz and 2500 Hz) used here, which are likely to favor ablation mechanisms.

The influence of laser repetition rate on  $I_{OLZ}$  was more complex, with the higher repetition rate increasing  $I_{OLZ}$  at all pulse energies for DHB, but for CHCA, a crossover is evident above 1.8  $\mu\text{J}$  pulse energy. Comparison with the number of

molecules desorbed (Figure 2d) suggests greater material ejection may explain some of the observed  $I_{OLZ}$  increase in DHB, whereas for CHCA, other effects are clearly occurring. Given the layered nature of the samples, a depth-of-sampling effect is possibly also influencing the data in some instances, especially at the lower pulse energies where full penetration of the matrix layer is not achieved (Figure 2b).

Changes to crater geometry are an important factor to consider for UV-MALDI MSI experiments, particularly if an oversampling or continuous raster acquisition mode is employed. CLSM measurements were used to determine the crater geometries under different pulse energies and repetition rates for both matrix compounds (Figure 2a). Differences between the matrix compounds, arising from their physicochemical properties, can be observed. For the same delivered pulse energy, DHB exhibited crater areas approximately 50% smaller than CHCA (Figure S3). This is likely due to DHB having significantly weaker absorption at the wavelength of the laser (355 nm) [50], thus having less energy available to drive material ejection. The change in crater size with pulse energy was less pronounced for DHB (Figure 2a). Overall crater shape remained somewhat symmetrical for this matrix, unlike CHCA

which evidenced significant elongation along the axis of the incident laser beam at higher pulse energies (Figure 2a). This suggests that DHB is more robust to the variations in energy distribution within the laser spot and changes in pulse energy, and so less likely to suffer from spatial resolution issues associated with Gaussian beam profiles. Although DHB is well known to form larger crystals than CHCA, which may serve to counteract this effect in many experiments, particularly those using solvent spray-based matrix depositions. Alternatively, the use of homogeneous beam profiles [42] could be used to negate these effects.

Despite noticeable differences on olanzapine ion intensity ( $I_{OLZ}$ ) between the two laser repetition rates (Figure 2b), the impact on crater geometry was far less pronounced, with crater areas effectively the same for both repetition rates (Figure S3). A small increase in material ejection at the higher repetition rate with DHB (Figure 2d) might explain the differences in  $I_{OLZ}$  for this matrix, pointing to sampling depth effects. This also suggests that variation in laser repetition rate is less of a concern for spatial resolution, but can have an influence on limits of detection.

For lasers with a Gaussian energy distribution, typically used in UV-MALDI MSI, heterogeneous ejection of material is to be expected within the irradiated sample area. The collected crater topography data allows us to quantify this effect under the conditions studied. Using knowledge of the matrix layer thickness, the threshold height for the crater edge detection algorithm was adjusted to be just above the substrate, allowing the region within a crater where the matrix layer was completely ejected to be identified (Figure 3a). By taking the ratio of crater volume bounded by this region to that of the full crater volume, we can provide an estimate of the efficiency of sampling ( $S_{EFF}$ ) under the studied conditions (Figure 3b–d). Within the limits imposed by UV-MALDI MS ionization dynamics and analyte extraction into the matrix layer, this metric describes the degree to which the ejected matrix is reflective of the underlying sample region, with a  $S_{EFF}$  of 100% corresponding to complete measurement. As such,  $S_{EFF}$  should have a direct impact to both the limits of detection of UV-MALDI analyses and on spatial resolution.

In spot mode,  $S_{EFF}$  increased with pulse energy, reaching a maximum of 80% for DHB and 70% for CHCA (Figure 3b). Based purely on material ejection, DHB could be seen as a superior matrix for lower limits of detection and higher spatial resolution with Gaussian profile beams, as its higher achievable  $S_{EFF}$  ensures maximal consumption of analyte within the matrix layer for given irradiated region. Although as previously noted, this matrix has a tendency to form large crystals, potentially counteracting any benefit in spatial resolution.

A  $S_{EFF}$  of up to  $\sim 90\%$  was observed in raster mode, with higher laser pulse energy and repetition rate improving  $S_{EFF}$ , and increased raster speed reducing it (Figure 3c and d). This was likely due to effective material ejection requiring sufficient laser energy and/or number of pulses per unit area. The higher  $S_{EFF}$  in raster mode compared to spot mode may be due to the shorter duration a specific area is irradiated, minimizing

material ejection in the low energy fringes of the laser spot material. These results suggest that on top of evident improvements in acquisition time, modest gains in limits of detection and spatial resolution can be made from adopting raster mode sampling over spot mode.

### *Ion Yields in MSI*

The absolute values of ion yields are a widely debated topic, with proposed values ranging from  $10^{-1}$  to  $10^{-8}$  for analyte ions and  $10^{-3}$  to  $10^{-9}$  for matrix ions. To date, there has been no investigation into how ion yields are affected by recent UV-MALDI MSI developments, namely the use of high laser repetition rates and continuous raster mode acquisition. By combining the measurements of material ejection with the corresponding MS data, we can provide estimates for olanzapine ion yield ( $Y_{OLZ}$ ) (Figure 4) and total ion yield ( $Y_{TIC}$ ) (Figure S5) under the conditions studied. It should be noted that due to simplifications made when estimating  $Y_{TIC}$ , these values should be considered a first-order approximation. For additional information, a comprehensive overview of acquired measurements relating to material ejection and ionization can also be found in Figure S2.

Ion yields for olanzapine ( $Y_{OLZ}$ ) ranged from  $10^{-9}$  to  $10^{-6}$ , which is towards the lower end of reported analyte values [28]. The total ion yield ( $Y_{TIC}$ ) ranged from  $10^{-10}$  to  $10^{-7}$  (Figure S5). While this may seem counter-intuitive, matrix ion yield is known to be orders of magnitude smaller than that of analytes [28]. As the matrix was the main contributor to the TIC here, besides the analyte, the total ion yield can be expected to be a convolution of the two components. In line with previous reports [51, 56], ion yields generally increased with pulse energy (Figure 4 and Figure S5), although given the layered nature of the samples, yields at lower pulse energies will also likely exhibit sampling depth effect for the analyte. The relative stability of  $Y_{OLZ}$  across higher pulse energies with CHCA is worthy of note for imaging experimentation, suggesting that there is a broad window of pulse energies before fragmentation begins to adversely affect ion yield. It is expected that DHB will also show a similar plateau region, but the range of pulse energies used here was not sufficient to access this regime. A small decrease in  $Y_{OLZ}$  was evident with CHCA at higher pulse energies for 2000 Hz in spot mode and 500 Hz,  $8 \text{ mm s}^{-1}$  in raster mode (Figure 4a and c); this matrix also showed significant drops in total ion yields at pulse energies above  $1.8 \mu\text{J}$  under nearly all conditions (Figure S5). Higher laser repetition rate was found to enhance  $Y_{OLZ}$  obtained with DHB in spot mode (Figure 4a), as more efficient sampling of the matrix layers can be ruled out due to similar observed  $S_{EFF}$  values (Figure 3a); this is likely due to enhanced material ejection, as the material ejection was also higher (Figure 2c).

In raster mode, the combinations of repetition rate and raster speed produced resulted in somewhat counter-intuitive behavior for both matrices (Figure 4b and c, Figure S5); for the faster raster speed, a higher repetition rate generally enhanced ion yield, but at the slower speed, a reduction was observed.



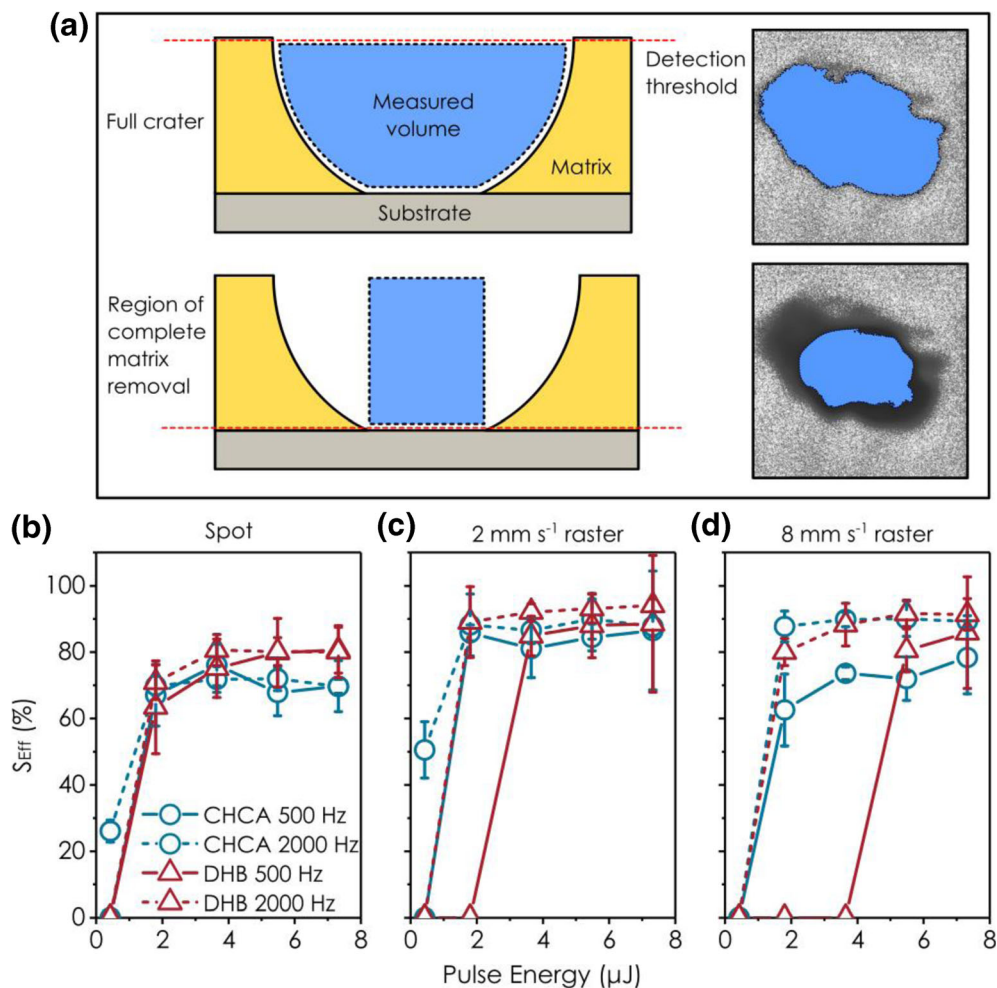


**Figure 3.** (a) Overview of sampling efficiency ( $S_{\text{Eff}}$ ) concept and measurement. Diagrams on the left show a cross-sectional view of how the full crater (top) and region of complete matrix ejection (bottom) volumes are determined; images on the right show the process with real crater data (CHCA, 500 Hz, 5.5  $\mu\text{J}$ ). Change in  $S_{\text{Eff}}$  with laser pulse energy for CHCA and DHB at 500 Hz and 2000 Hz, for (b) spot mode, (c) 2 mm s<sup>-1</sup> raster, and (d) 8 mm s<sup>-1</sup> raster

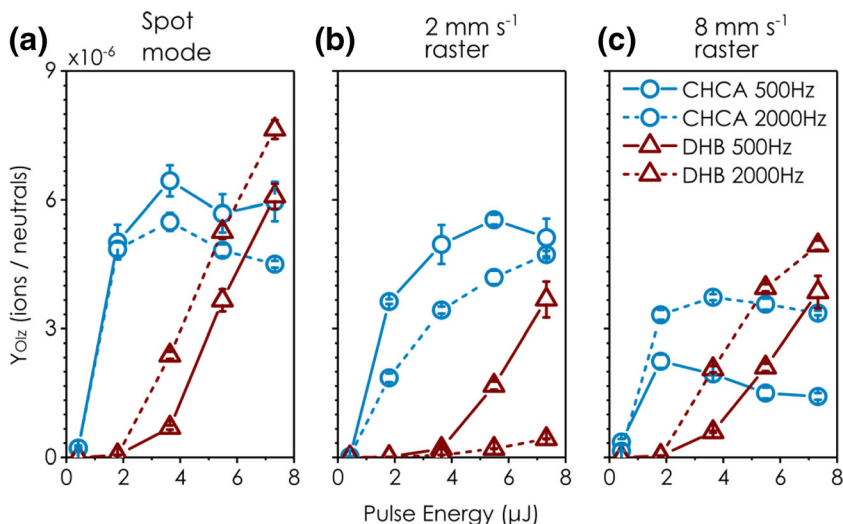


**Figure 4.** Ion yield of olanzapine ( $Y_{\text{OLZ}}$ ) with increasing pulse energy under different imaging conditions. (a) Spot mode acquisition. (b) 2 mm s<sup>-1</sup> raster. (c) 8 mm s<sup>-1</sup> raster. All raster data is normalized to pixel size. Error bars show the expanded uncertainty ( $k = 2$ )

Additionally, the trend of ion yield with pulse energy seemed to shift towards higher pulse energies when the higher repetition rate was employed, and towards lower pulse energies with faster raster speed. Previously reported work from our lab has observed similar trends for CHCA in thin film and tissue samples, where optimal pulse energies for highest ion intensities shifted with repetition rate and raster speed [41]. The associated ejected material data suggests that these trends were a product of ion formation or ejection plume mechanisms, as they were evident in both the olanzapine and TIC data (Figure S5), but not in the amount of desorbed material (Figure S4). Although in the case of the latter measurement, there may be changes in ablation occurring at the leading edge of the laser beam which could not be captured in these experiments.

As the raster speed and repetition rate conditions studied here both differed by a factor of four, the 500 Hz, 2 mm s<sup>-1</sup> and 2000 Hz, 8 mm s<sup>-1</sup> raster data both resulted in an equivalent irradiation condition of four pulses delivered for every micrometer of raster travel. This enables the effect of repetition rate in raster mode to be isolated from the other conditions (Figure 5).

Under these equivalent pulse number conditions, large differences in  $Y_{OLZ}$  and  $Y_{TIC}$  between repetition rates were evident (Figure 5 and Figure S6), producing similar results to that obtained in spot mode (Figure 4a). The only parameter that differs between the two conditions was the time between laser pulses, which was 2 ms at 500 Hz and 500  $\mu$ s at 2000 Hz. This dependence of ion yield on time between delivered pulses was previously observed for detected ion intensities with CHCA [41], which found that ion signals for lipid species generally decreased with increasing repetition rate. Here, we can extend these findings to measurements of ion yield, and with an additional matrix and a different analyte. Interestingly, while the

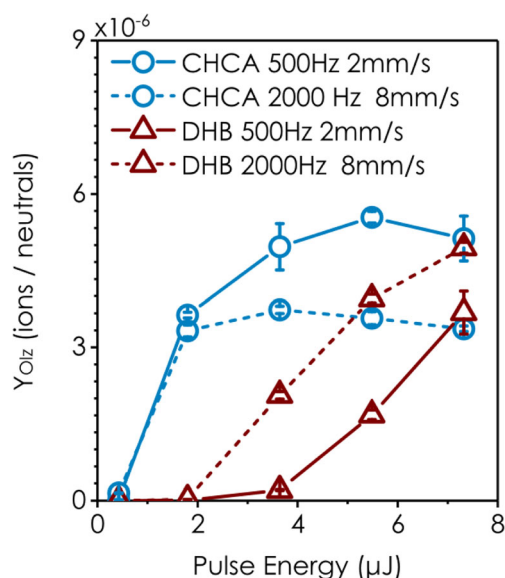


**Figure 5.** Change in olanzapine ion yield ( $Y_{OLZ}$ ) with pulse energy under equivalent irradiation conditions. Data shows raster mode acquisitions where the raster speed and laser repetition rate conditions resulted in four pulses delivered per micrometer of travel. All data is normalized to pixel size

CHCA results agree with those previous findings, the current results show that DHB behaves in completely the opposite manner (Figure 5 and Figure S6). We postulate two potential causes for this effect, which could either occur individually, or more likely in parallel, during raster mode acquisitions.

Firstly, given the Gaussian energy distribution of the laser, irradiated matrix volumes at the periphery of the laser spot will be heated but not sufficiently to result in ejection of material. It has been previously shown that sample temperature has a direct impact on material ejection in UV-MALDI and release of ions for detection [57]. At the time of arrival of a subsequent pulse, the extent of the heated volume would be dependent on matrix properties such as optical absorption, heat capacity, and thermal diffusion. The fivefold difference in optical absorption at 355 nm between the two matrices [50, 58] will mean that this heated volume will be more extensive for the weakly absorbing DHB. Thermal diffusivity, which is a measure of the rate of heat transfer through a material, is not known for the matrices used here, but is typically in the range on 10<sup>-7</sup> m<sup>2</sup> s<sup>-1</sup> for molecular solids [59]. Over the inter-pulse timescales in Figure 5 (500  $\mu$ s to 2 ms), heat induced by the laser will have traveled approximately 4–8  $\mu$ m from the edge of the irradiated region. This is of same order as the distance between pulses (4  $\mu$ m), suggesting that any residual heat imparted by a preceding pulse, will likely contribute to material ejection from the next pulse.

Secondly, CHCA is known to exhibit what is termed the “shot effect,” whereby the ion signal from a fixed sample position decreases with successive laser shots, theorized to be resulting from a mixture of photochemical-induced [60] and thermochemical-induced changes in the matrix [41]. It has been reported that while DHB is more stable, CHCA readily undergoes a variety of reactions upon melting, resulting in a reduction of absorption at 355 nm and an increase in fluorescence emission intensity [61], both of which are known to reduce detected ion intensities in UV-MALDI MS [22, 43, 62, 63]. The decrease in  $Y_{OLZ}$  with CHCA when operating at the higher repetition rate may then be a result of increased photo- and thermo-degradation of the matrix within the irradiated area, potentially further evidenced by the previous observed zones in the AFM phase data for this matrix (Figure 1b). This would further explain why the trend in ion yields (Figure 5) for this matrix did not correlate with amount of material ejected (Figure S4).

The results show that raster mode is able to achieve a similar degree of limits of detection to spot mode, as long as an appropriate pulse energy and repetition rate are used. Although care must be taken, optimizing these parameters as they are not consistent across different raster speeds and behavior is highly dependent on the matrix employed.

## Conclusions

By using well-defined model systems and volumetric measurements of material ejection, we demonstrate absolute ion yield measurements under a range of different UV-MALDI MSI sampling conditions. To the authors’ knowledge, this is the



first study to report on absolute ion yields in UV-MALDI MSI, and should serve as a useful aid for the optimization of acquisition parameters in UV-MALDI MS imaging experiments.

We determine that analyte ion yields for the systems studied span approximately  $10^{-9}$  to  $10^{-6}$  ions per desorbed molecule, supporting more recent lower estimates of UV-MALDI MS ion yields. Better characterization of commercial MSI instruments would enable more accurate measurements of ion yield to be conducted in the future, and a thorough inter-comparison of commonly used instrumentation in UV-MALDI MSI, and MSI in general, would be of great use to the wider community. Additionally, to gain a clearer picture of complex behaviors evidenced by our results, it would be useful to extend these measurements, incorporating a wider range of pulse energies, repetition rates, and raster speeds, as well additional matrix compounds and analytes. Inclusion of other relevant UV-MALDI MSI experimental parameters such as laser spot size, beam profile, and oversampling mode acquisition would also be highly informative. The observed similarities in ion yield between raster and spot mode provide assurance to UV-MALDI MSI users that continuous raster acquisition mode can be utilized with little impact to limits of detection, as long as appropriate steps are taken to ensure suitable laser parameters are applied. This caveat highlights the benefits proper knowledge of laser conditions can provide to optimization of UV-MALDI MS imaging experiments.

The significant observed differences in material ejection between the studied conditions suggest that beyond widely accepted influences on resolution (laser spot size, step size, matrix crystal size, and degree of analyte delocalization), other factors such as properties of the matrix utilized, laser pulse energy, repetition rate, and beam profile can have significant effects. In particular, proposed definitions for image resolution in UV-MALDI MSI relying on only one or a few of these conditions are in danger of over-simplifying a highly complex process. The results highlight the drawbacks of using lasers with Gaussian beam profiles, and suggest that the adoption of more suitable beam profiles should be seriously considered.

Because there are known differences in matrix behavior between thin film systems, like those studied here, and matrix on tissue, it is necessary to further explore the results obtained here in a tissue imaging context. With this in mind, a series of experiments are underway to determine the influence of sampling parameters on ion yields and image resolution in UV-MALDI MS imaging of tissues.

## Acknowledgements

The authors would like to thank Steve Pringle (Waters) for assistance in determination of Synapt ion transmission efficiencies, Wenjuan Sun (NPL) for providing access and training for the CLSM, Charles Clifford (NPL) for AFM access and training, and Ken Mingard (NPL) for providing access to SEM. Funding for the work presented here was provided through the AIMS HIGHER project as part of the NPL strategic research program.

## References

- Greer, T., Sturm, R., Li, L.: Mass spectrometry imaging for drugs and metabolites. *J. Proteome*. **74**, 2617–2631 (2011)
- Bonk, T., Humeny, A.: MALDI-TOF-MS analysis of protein and DNA. *Neuroscientist*. **7**, 6–12 (2001)
- Li, L.: Overview of MS and MALDI MS for polymer analysis. In: *Maldi mass spectrometry for synthetic polymer analysis*, pp. 1–8. John Wiley & Sons, Inc., Hoboken (2009)
- Amstalden van Hove, E.R., Smith, D.F., Heeren, R.M.A.: A concise review of mass spectrometry imaging. *J. Chromatogr. A*. **1217**, 3946–3954 (2010)
- Balluff, B., Schöne, C., Höfler, H., Walch, A.: MALDI imaging mass spectrometry for direct tissue analysis: technological advancements and recent applications. *Histochem. Cell Biol.* **136**, 227–244 (2011)
- Castellino, S., Groseclose, M.R., Wagner, D.: MALDI imaging mass spectrometry: bridging biology and chemistry in drug development. *Bioanalysis*. **3**, 2427–2441 (2011)
- Dreisewerd, K.: The desorption process in MALDI. *Chem. Rev.* **103**, 395–426 (2003)
- Niehaus, M., Soltwisch, J.: New insights into mechanisms of material ejection in MALDI mass spectrometry for a wide range of spot sizes. *Sci. Rep.* **8**, 7755 (2018)
- Knochenmuss, R., Zhigilei, L.V.: Molecular dynamics simulations of MALDI: laser fluence and pulse width dependence of plume characteristics and consequences for matrix and analyte ionization. *J. Mass Spectrom.* **45**, 333–346 (2010)
- Soltwisch, J., Jaskolla, T.W., Dreisewerd, K.: Color matters—material ejection and ion yields in UV-MALDI mass spectrometry as a function of laser wavelength and laser fluence. *J. Am. Soc. Mass Spectrom.* **24**, 1477–1488 (2013)
- Phipps, C.: *Laser ablation and its applications*. Springer US, Boston (2007)
- Sadeghi, M., Vertes, A.: Crystallite size dependence of volatilization in matrix-assisted laser desorption/ionization. *Appl. Surf. Sci.* **127–129**, 226–234 (1998)
- Puretzky, A.A., Geohegan, D.B.: LIF imaging and gas-phase diagnostics of laser desorbed MALDI-matrix plumes. *Appl. Surf. Sci.* **127–129**, 248–254 (1998)
- Rohlfing, A., Leisner, A., Hillenkamp, F., Dreisewerd, K.: Investigation of the desorption process in UV matrix-assisted laser desorption/ionization with a liquid 3-nitrobenzyl alcohol matrix by photoacoustic analysis, fast-flash imaging, and UV-laser postionization. *J. Phys. Chem. C*. **114**, 5367–5381 (2010)
- Schmitz, T.A., Koch, J., Günther, D., Zenobi, R.: Early plume and shock wave dynamics in atmospheric-pressure ultraviolet-laser ablation of different matrix-assisted laser ablation matrices. *J. Appl. Phys.* **109**, 123106 (2011)
- Boekelmann, V., Spengler, B., Kaufmann, R.: Dynamical parameters of ion ejection and ion formation in matrix-assisted laser desorption/ionization. *Eur. Mass Spectrom.* **1**, 81–93 (1995)
- Ellis, S.R., Soltwisch, J., Heeren, R.M.A.: Time-resolved imaging of the MALDI linear-TOF ion cloud: direct visualization and exploitation of ion optical phenomena using a position- and time-sensitive detector. *J. Am. Soc. Mass Spectrom.* **25**, 809–819 (2014)
- Strupat, K., Karas, M., Hillenkamp, F.: 2,5-Dihydroxybenzoic acid: a new matrix for laser desorption—ionization mass spectrometry. *Int. J. Mass Spectrom. Ion Process.* **111**, 89–102 (1991)
- Westman, A., Huth-Fehre, T., Demirev, P., Sundqvist, B.U.R.: Sample morphology effects in matrix-assisted laser desorption/ionization mass spectrometry of proteins. *J. Mass Spectrom.* **30**, 206–211 (1995)
- Fournier, I., Beavis, R.C., Blais, J.C., Tabet, J.C., Bolbach, G.: Hysteresis effects observed in MALDI using oriented, protein-doped matrix crystals. *Int. J. Mass Spectrom. Ion Process.* **169–170**, 19–29 (1997)
- Kampmeier, J., Dreisewerd, K., Schürenberg, M., Strupat, K.: Investigations of 2,5-DHB and succinic acid as matrices for IR and UV MALDI. Part I UV and IR laser ablation in the MALDI process. *Int. J. Mass Spectrom. Ion Process.* **169–170**, 31–41 (1997)
- Wiegelmann, M., Soltwisch, J., Jaskolla, T.W., Dreisewerd, K.: Matching the laser wavelength to the absorption properties of matrices increases the ion yield in UV-MALDI mass spectrometry. *Anal. Bioanal. Chem.* **405**, 6925–6932 (2013)

23. Fournier, I., Tabet, J., Bolbach, G.: Irradiation effects in MALDI and surface modifications. *Int. J. Mass Spectrom.* **219**, 515–523 (2002)
24. Fournier, I., Marinach, C., Tabet, J.C., Bolbach, G.: Irradiation effects in MALDI, ablation, ion production, and surface modifications. Part II: 2,5-dihydroxybenzoic acid monocrystals. *J. Am. Soc. Mass Spectrom.* **14**, 893–899 (2003)
25. Spengler, B., Hubert, M.: Scanning microprobe matrix-assisted laser desorption/ionization (SMALDI) mass spectrometry: instrumentation for sub-micrometer resolved LDI and MALDI surface analysis. *J. Am. Soc. Mass Spectrom.* **13**, 735–748 (2002)
26. Moon, J.H., Shin, Y.S., Bae, Y.J., Kim, M.S.: Ion yields for some salts in MALDI: mechanism for the gas-phase ion formation from preformed ions. *J. Am. Soc. Mass Spectrom.* **23**, 162–170 (2012)
27. Bae, Y.J., Shin, Y.S., Moon, J.H., Kim, M.S.: Degree of ionization in MALDI of peptides: thermal explanation for the gas-phase ion formation. *J. Am. Soc. Mass Spectrom.* **23**, 1326–1335 (2012)
28. Tsai, M.T., Lee, S., Lu, I.C., Chu, K.Y., Liang, C.W., Lee, C.H., Lee, Y.T., Ni, C.K.: Ion-to-neutral ratio of 2,5-dihydroxybenzoic acid in matrix-assisted laser desorption/ionization. *Rapid Commun. Mass Spectrom.* **27**, 955–963 (2013)
29. Ahn, S.H., Park, K.M., Bae, Y.J., Kim, M.S.: Quantitative reproducibility of mass spectra in matrix-assisted laser desorption/ionization and unraveling of the mechanism for gas-phase peptide ion formation. *J. Mass Spectrom.* **48**, 299–305 (2013)
30. Bae, Y.J., Park, K.M., Kim, M.S.: Reproducibility of temperature-selected mass spectra in matrix-assisted laser desorption/ionization of peptides. *Anal. Chem.* **84**, 7107–7111 (2012)
31. Bae, Y.J., Choe, J.C., Moon, J.H., Kim, M.S.: Why do the abundances of ions generated by MALDI look thermally determined? *J. Am. Soc. Mass Spectrom.* **24**, 1807–1815 (2013)
32. Knochenmuss, R.: MALDI ionization mechanisms: the coupled photophysical and chemical dynamics model correctly predicts ‘temperature’-selected spectra. *J. Mass Spectrom.* **48**, 998–1004 (2013)
33. Chu, K.Y., Lee, S., Tsai, M.T., Lu, I.C., Dyakov, Y.A., Lai, Y.H., Lee, Y.T., Ni, C.K.: Thermal proton transfer reactions in ultraviolet matrix-assisted laser desorption/ionization. *J. Am. Soc. Mass Spectrom.* **25**, 310–318 (2014)
34. Knochenmuss, R.: Energetics and kinetics of thermal ionization models of MALDI. *J. Am. Soc. Mass Spectrom.* **25**, 1521–1527 (2014)
35. Lu, I.-C., Chu, K.-Y., Lin, C.-Y., Wu, S.-Y., Dyakov, Y.a., Chen, J.-L., Gray-Weale, A., Lee, Y.-T., Ni, C.-K.: Ion-to-neutral ratios and thermal proton transfer in matrix-assisted laser desorption/ionization. *J. Am. Soc. Mass Spectrom.* **26**, 1242–1251 (2015)
36. Knochenmuss, R.: Ion yields in the coupled chemical and physical dynamics model of matrix-assisted laser desorption/ionization. *J. Am. Soc. Mass Spectrom.* **26**, 1645–1648 (2015)
37. Knochenmuss, R.: The coupled chemical and physical dynamics model of MALDI. *Annu. Rev. Anal. Chem.* **9**, 365–385 (2016)
38. Dreisewerd, K., Schürenberg, M., Karas, M., Hillenkamp, F.: Matrix-assisted laser desorption/ionization with nitrogen lasers of different pulse widths. *Int. J. Mass Spectrom. Ion Process.* **154**, 171–178 (1996)
39. Liang, S.-P., Lu, I.-C., Tsai, S.-T., Chen, J.-L., Lee, Y.T., Ni, C.-K.: Laser pulse width dependence and ionization mechanism of matrix-assisted laser desorption/ionization. *J. Am. Soc. Mass Spectrom.* **28**, 2235–2245 (2017)
40. Spraggins, J.M., Caprioli, R.M.: High-speed MALDI-TOF imaging mass spectrometry: rapid ion image acquisition and considerations for next generation instrumentation. *J. Am. Soc. Mass Spectrom.* **22**, 1022–1031 (2011)
41. Steven, R.T., Dexter, A., Bunch, J.: Investigating MALDI MSI parameters (part 1) – a systematic survey of the effects of repetition rates up to 20kHz in continuous raster mode. *Methods.* **104**, 101–110 (2016)
42. Wiegmann, M., Dreisewerd, K., Soltwisch, J.: Influence of the laser spot size, focal beam profile, and tissue type on the lipid signals obtained by MALDI-MS imaging in oversampling mode. *J. Am. Soc. Mass Spectrom.* **27**, 1952–1964 (2016)
43. Niehaus, M., Schnapp, A., Koch, A., Soltwisch, J., Dreisewerd, K.: New insights into the wavelength dependence of MALDI mass spectrometry. *Anal. Chem.* **89**, 7734–7741 (2017)
44. Steven, R.T., Palmer, A.D., Bunch, J.: Fluorometric beam profiling of UV MALDI lasers. *J. Am. Soc. Mass Spectrom.* **24**, 1146–1152 (2013)
45. Nečas, D., Klapetek, P.: Gwyddion: an open-source software for SPM data analysis. *Open Phys.* **10**, 181–188 (2012)
46. Race, A.M., Styles, I.B., Bunch, J.: Inclusive sharing of mass spectrometry imaging data requires a converter for all. *J. Proteome.* **75**, 5111–5112 (2012)
47. Race, A.M., Palmer, A.D., Dexter, A., Steven, R.T., Styles, I.B., Bunch, J.: SpectralAnalysis: software for the masses. *Anal. Chem.* **88**, 9451–9458 (2016)
48. Jaskolla, T.W., Karas, M., Roth, U., Steinert, K., Menzel, C., Reihls, K.: Comparison between vacuum sublimed matrices and conventional dried droplet preparation in MALDI-TOF mass spectrometry. *J. Am. Soc. Mass Spectrom.* **20**, 1104–1114 (2009)
49. Cleveland, J.P., Anczykowski, B., Schmid, A.E., Elings, V.B.: Energy dissipation in tapping-mode atomic force microscopy. *Appl. Phys. Lett.* **72**, 2613–2615 (1998)
50. Robinson, K.N., Steven, R.T., Bunch, J.: Matrix optical absorption in UV-MALDI MS. *J. Am. Soc. Mass Spectrom.* **29**, 501–511 (2018)
51. Westmacott, G., Ens, W., Hillenkamp, F., Dreisewerd, K., Schürenberg, M.: The influence of laser fluence on ion yield in matrix-assisted laser desorption/ionization mass spectrometry. *Int. J. Mass Spectrom.* **221**, 67–81 (2002)
52. Qiao, H., Spicer, V., Ens, W.: The effect of laser profile, fluence, and spot size on sensitivity in orthogonal-injection matrix-assisted laser desorption/ionization time-of-flight mass spectrometry. *Rapid Commun. Mass Spectrom.* **22**, 2779–2790 (2008)
53. Steven, R.T., Race, A.M., Bunch, J.: Probing the relationship between detected ion intensity, laser fluence, and beam profile in thin film and tissue in MALDI MSI. *J. Am. Soc. Mass Spectrom.* **27**, 1419–1428 (2016)
54. Zhigilev, L.V., Garrison, B.J.: Microscopic mechanisms of laser ablation of organic solids in the thermal and stress confinement irradiation regimes. *J. Appl. Phys.* **88**, 1281–1298 (2000)
55. Jackson, S.N., Mishra, S., Murray, K.K., Jackson, S.N., Mishra, S., Murray, K.K.: Characterization of coarse particles formed by laser ablation of MALDI matrixes. *J. Phys. Chem. B.* **107**, 13106–13110 (2003)
56. Westman, A., Huth-Fehre, T., Demirev, P., Bielawski, J., Medina, N., Sundqvist, B.U.R., Karas, M.: Matrix-assisted laser desorption/ionization: dependence of the ion yield on the laser beam incidence angle. *Rapid Commun. Mass Spectrom.* **8**, 388–393 (1994)
57. Schürenberg, M., Dreisewerd, K., Kamanabrou, S., Hillenkamp, F.: Influence of the sample temperature on the desorption of matrix molecules and ions in matrix-assisted laser desorption/ionization. *Int. J. Mass Spectrom. Ion Process.* **172**, 89–94 (1998)
58. Allwood, D.a., Dreyfus, R.W., Perera, I.K., Dyer, P.E.: UV optical absorption of matrices used for matrix-assisted laser desorption/ionization. *Rapid Commun. Mass Spectrom.* **10**, 1575–1578 (1996)
59. Koubenakis, A., Frankevich, V., Zhang, J., Zenobi, R.: Time-resolved surface temperature measurement of MALDI matrices under pulsed UV laser irradiation. *J. Phys. Chem. A.* **108**, 2405–2410 (2004)
60. Mesaros, M., Tarzi, O.I., Erra-Balsells, R., Bilmes, G.M.: The photophysics of some UV-MALDI matrices studied by using spectroscopic, photoacoustic and luminescence techniques. *Chem. Phys. Lett.* **426**, 334–340 (2006)
61. Tarzi, O.I., Nonami, H., Erra-Balsells, R.: The effect of temperature on the stability of compounds used as UV-MALDI-MS matrix: 2,5-dihydroxybenzoic acid, 2,4,6-trihydroxyacetophenone,  $\alpha$ -cyano-4-hydroxycinnamic acid, 3,5-dimethoxy-4-hydroxycinnamic acid, nor-harmaline and harmaline. *J. Mass Spectrom.* **44**, 260–277 (2009)
62. Setz, P.D., Knochenmuss, R.: Exciton mobility and trapping in a MALDI matrix. *J. Phys. Chem. A.* **109**, 4030–4037 (2005)
63. Soltwisch, J., Jaskolla, T.W., Hillenkamp, F., Karas, M., Dreisewerd, K.: Ion yields in UV-MALDI mass spectrometry as a function of excitation laser wavelength and optical and physico-chemical properties of classical and halogen-substituted MALDI matrixes. *Anal. Chem.* **84**, 6567–6576 (2012)